International Journal of Renewable Energy and Environmental Sustainability
Volume. 9, Number 4;October-December, 2024;
ISSN: 2837-3391| Impact Factor: 7.45
https://zapjournals.com/Journals/index.php/ijrees
Published By: Zendo Academic Publishing

DARK MATTER CAN BE REVEALED INSIDE THE EARTH BY STRING THEORY

[1]Hsien-Jung Ho
e-mail: newidea.ufoho@msa.hinet.net

Article Info
Keywords: Keywords: Dark matter, Multiverse, Density jump, Convection cell, Chandler wobble.

DOI
https://doi.org/10.5281/zenodo.13982835

Abstract
Applying the original String theory (ten-dimensional spacetime theory) to solve the problem of dark matter. According to "Causality Principle" and "Anthropic Principle", the universe may be divided into triple cosmoses, and dark matter should be considered as stars or planets in space other than ours. The best method for exploring dark matter is to start from Earth. According to the characteristics of the Earth' interior, by equitably examining its constitution, temperature, density, and pressure from a different perspective of the core, special arguments are put forward. The great amounts of heat produced from radiogenic heat, chemical reaction heat, and nuclear fission heat become the power sources for the geo-dynamo of great convection cells, which are the flows of magma and rock migrating up to the crust and down across the core-mantle boundary (CMB) to the F layer. Based on the new conception, Earth data are calculated and compared with current data. Insufficient mass and moment of inertia belong to dark matter. Apply a simplified method to evaluate the Earth's mass and moment of inertia, which were found to be only 85.73% and 94.82% of the current data, respectively. Due to the insufficiency of the Earth's data, a planet of dark matter, which is inside the Earth but other space than ours, has been calculated. The new conception may be confirmed by the Chandler wobble, and the problem of dark matter can be roughly solved.

1. Introduction

In 1937, Caltech astronomer Zwicky noticed that masses of nebulae were estimated either from the luminosities of nebulae or from their internal rotations and surmised that some extra, hidden mass must have been presented to supply gravitational glue [1]. In the 1970s, astronomers detected that when stars outside the edges of the Milky Way and other spiral galaxies were found to be orbiting faster than theory predict; individual galaxies seemed also harbored a reservoir of unseen matter whose gravity kept their stars from escaping[2]. The total mass of stars in a galaxy, which can be estimated by observing the galaxy with an astronomical telescope, is less than 10% of the total mass of the galaxy estimated from the orbiting stars. This phenomenon appears throughout the universe. Unobservable matter, which amounted to more than 90 % of the mass of the entire universe, is called dark matter [3]. Dark matter is real and can only be detected by its gravitational influence on visible matter. This is a major

[1] Host / Newidea Research Center, Address: 10 Floor, No. 110-6, Jie-Shou N Road, Changhua, Taiwan.

problem that still has no solution.

In 1998, the High-Z Supernova Search Team published observations of type 1asupernova as standard candles [4], and in 1999, the Supernova Cosmology Project was launched [5]. The two independent projects obtained results suggesting a totally unexpected acceleration in the expansion of the universe. In order to explain the phenomenon of the universe expanding at an accelerated rate, "dark energy" is the most accepted hypothesis for observation.

The cosmological parameters of Planck 2018 results VI were taken as the current situation of the universe, where dark energy remained 68.42% of the composition of the universe after the Big Bang, dark matter contained 26.64 %, and normal matter contained 4.94 % [6]. Dark energy is a current scientific hypothesis, which acts as a sort of anti-gravity and is responsible for the present-day acceleration of the Universal expansion, but it is neither matter nor radiation, its physical properties have no clue, and we do not know how it works, and dark matter is also no solution; therefore, now all astrophysicists take both as major problems today.

Scientists believe that dark energy is the force that tears the universe apart, that dark matter condenses all things, and that the interaction between these two forces forms the structure of the universe as we know it today. As long as we can understand the assembling speed of a galaxy, we can understand dark matter and also understand the power of dark energy tearing through the universe at the same time. Thus, dark matter may be the best tool to study dark energy. To understand dark matter at this time, we will probably get an answer from the most famous "String theory".

2. Multiverse Research Review

2.1 Ten-dimensional space-time of the original string theory reveals multiverse

In order to address these questions of astrophysics, in 1970s String theory was introduced. String theory begins with the notion that point like particles in particle physics can also be modeled as one-dimensional objects called strings. The characteristic length scale of strings is assumed to be on the order of Planck length, or 10^{-35} meters that looks just like an ordinary particle, with its mass, charge, and other properties determined by its vibrational states in different ways. In quantum field theory, when a string moving in the framework of time and space is so complex that three-dimensional space can no longer accommodate its motion orbit, there must be up to nine-dimensional space to meet the motion. Thus, all objects are considered as a nine-dimensional space of the string. The original String theory is based on the universe constitution of nine-dimensional space and one-dimensional time. The 10-dimensional space-time of String theory is interpreted as the product of ordinary 4-dimensional space-time and 6-extra-dimensional spaces, which have not been observed [7].

In the multidimensional theory of String theory, the force of gravity is the only force of nature that has effect across all dimensions. This explains the relative weakness of gravity compared to other forces of nature (as electromagnetic wave) that cannot cross into extra dimensions. In that case, dark matter could exist in extra-dimensional space, where it only interacts with matter in our space through gravity. Dark matter could aggregate in the same way as ordinary matter, forming extra-dimensional galaxies [8]. To date, experimental or observational evidence is not available to confirm the existence of these extra dimensions.

In 2004, Dvali suggested that the extra dimensions of space does not curl up (not compactified) becomes minimum, but infinite in size and uncurved, just like our ordinary three-dimensional view [9]. In particular, this theory predicts that the universe has extra dimensions into which gravity, unlike ordinary matter, can escape. This leakage would warp the space-time continuum and accelerate the cosmic expansion. Thus, the extra dimensions do not need to be small and compact, but may be large extra dimensions, i.e., outside our ordinary three-dimensional space, there are the same six extra dimensions of space in the universe.

According to "Causality", an effect cannot occur before its cause, which means that time has one direction and cannot be divided into different parts; therefore, one-dimensional time is taken as a common standard for the order of events in the universe. Following the "Anthropic Principle", which is the simple fact that we live in a universe set up to allow for our existence, three-dimensional space and one-dimensional time are taken as one cosmos, the living world. Therefore, the nine-dimensional space can be divided into three portions, each of which has a common time standard. This means that there is a 3-cosmic framework in the universe, called triple cosmoses, i.e., multiverse, which cannot be observed directly with one another.

2.2. A multiverse theory

In 1982, American physicist Alan Guth, who studied cosmology, proposed inflation theory, which explained that the universe expanded at a very rapid rate of geometric progression, and the volume expanded by a hundred thousand times in an instant after the Big Bang. When the expansion stops, it will not stop completely at the same time. In some places, it will stop, and those places will become the universe. In other places, the expansion will continue. Later, more small universes will form, and countless small universes may form. We now call them multiverses, and this process is called permanent expansion; therefore, there are innumerable universes, not just one universe we see [10]. The multiverse is a hypothetical group of multiple universes.

In 1957, Princeton University Everett devised "the many-worlds interpretation (MWI) of quantum mechanics" [11]. The core of the idea is to interpret in the quantum world that an elementary particle, or a collection of such particles, can exist in a superposition of two or more possible states of being. An electron, for example, can be in a superposition of different locations, velocities, and orientations of its spin. However, whenever scientists measure one of these properties with precision, they obtain a definite result—just an element of the superposition, not a combination of them. No macroscopic objects are observed in superposition. The many-world interpretation is a multiverse theory [12].

String theory states that the three-cosmic framework of the universe has characteristics in which each cosmos describes a world of general matter, whereas the others describe another world that we know nothing. Among any another cosmos, there are no basic interactive forces of nature except gravity; in other words, theoretic gravitons in the field of gravity can penetrate all three cosmoses; however, light (electromagnetic wave) cannot, meaning that dark matter may exist in cosmoses other than ours. The best method for exploring dark matter is to start from Earth, where we live.

3. Materials and Methods

3.1 Multiverse exploration of dark matter from Earth

In the current Earth model utilized in seismological investigations, such as body-wave travel times, surface- wave dispersion, and free oscillation periods for researching the chemical composition and density distribution of the Earth, the portions of the crust and the upper mantle have been analyzed with satisfactory accuracy. However, regarding the lower mantle and core, a number of questions remain to be answered. It has been well known that there are two convections circulating individually below the crust to the lower mantle and in the outer core itself. The mantle and core are not in chemical equilibrium, and the fine structure of the core-mantle boundary (CMB) is not well understood. Although some hypotheses such as the existence of a D″ layer in the lower mantle and iron combined with oxygen as the primary alloying constituent of the outer core have been suggested, and a lot of advances in this research have come out, there are also some discrepancies in the interior of the Earth [13]. Furthermore, there is no conclusive evidence that the inner core is in thermodynamic equilibrium with the outer core.

The main problem is the lack of phase-equilibrium data for plausible core compositions under the appropriate conditions, added to the fact that seismological observations do not yet offer a decisive constraint on the difference in composition between the inner and outer core [14]. To investigate the outer core, a different view of the deep interior of the Earth should be taken to analyze the Earth's constitution, composition, temperature, and pressure, and a revolution in its chemical composition should be developed.

3.2 Arguments at core mantle boundary

With regard to the Earth's interior, the constitution of the deep interior is uncertain, and there are some difficulties. To conduct further investigations, the Preliminary Reference Earth Model (PREM) [15] was taken as the current Earth model in this paper. There are arguments in the topic of CMB as in the following: 1. In 1948, Ramsey[16] and in 1973, Lyttleton [17] challenged the concept of an iron core, stating that the CMB is the boundary of Ramsey's phase change, not the silicates and iron core interface. 2. In 1965, Knopoff [18] showed that the bulk modulus remains constant so that the density distribution is continuous at the CMB. 3. In 1968, Buchbinder [19] studied the variation in the reflection amplitudes of seismic waves and found that they show a phase change at the CMB.

From items 1, 2, and 3 above, it can be initially identified that the materials of mantle and core mix with each other, and the density distribution between the lower mantle and the outer core should be consistent to solve some geophysics problems. The main components of the outer core should be considered as the same ingredients of molten rock and/or mineral silicates, which are chemically consistent with the ingredients found the lowermost mantle.

3.3 The topography of the CMB revealed that both sides were made of the same materials

A sufficient quantity of high-quality digital data from two global networks: a network for very long-term seismology [20] and a seismic research observatory [21], which began operation in the mid-1970s and developed over four decades, provided the framework of formal analysis. The availability of computers made the handling of immense amounts of data feasible and the large-scale calculations necessary for three-dimensional problems. Geophysicists recorded on Earth more than 15,000 times magnitude 4.5th-class earthquake data, input a seismic laboratory computer, drawn a three-dimensional topographical map of the Earth's Interior, and produced computer tomography X-ray photographs, producing the CMB topography, which is found in boundary of solid mantle and liquid outer core. Maps of the CMB topography have been derived on the basis of seismological inversions of long-wave travel times to construct three-dimensional maps with the magnitude of amplitudes from ±3 km up to ±6 km (largest relief 12 km) and with 3000～6000 km scale lengths [22-33].

In three-dimensional maps of the Earth's interior, the topography of the CMB differs from that predicted by hydrostatic equilibrium theory, which contains information important to geodynamic processes and geomagnetic secular variation. The topography of the CMB is likely due to convection in the overlying mantle [34]. In 1980, Ruff and Anderson argued for dynamo action in the core maintained by differential heating of the core by the mantle [35], and some agreements with them were probably determined by processes in the core [36]. The depressed regions of the topography are dynamically supported by down welling of cool mantle material [37], indicating that the relief is dynamically supported and provides coupling between the solid mantle and the fluid core. Scientists suggest further effects due to topography associated with subduction slabs, which may have a mechanical rather than thermal effect on the flow [38].

It is obvious in terms of geodynamic processes that only the vertical interactions of the material and the temperature between the lowermost mantle and the outer core are the main causes. In order to maintain the 10 km of relief, the density difference between the liquid and solid states at the CMB must be very small, so the density of the materials between both sides at the CMB must be similar or equal, i.e., the hypothesis that the same materials between the solid mantle and liquid core change state with each other at the CMB.

3.4 Heat flow of core leaks into mantle

In 1971, geophysicist Morgan proposed the hypothesis of mantle plumes, which are generated from thermal boundary layers and have been invoked for decades to explain the formation of hotspots and flood basalt provinces on Earth [39]. In this hypothesis, convection in the mantle transports heat from the core to the Earth's surface in thermal diapirs. There are two largely independent convective processes occurring in the mantle. 1. *Mantle plumes* carry heat upward in narrow, rising columns driven by heat exchange across the core-mantle boundary to the crust. 2. The broad convective flow associated with *plate tectonics* is driven primarily by sinking the cold plates of the lithosphere back into the mantle [40].

Mantle plumes are tubes of hot rock rising from Earth's core, many of which lie underneath known volcanic hot spots at Earth's surface. The thermal plumes are fatter than expected, meaning that they carry more heat away from the Earth core, indicating that plumes are important for cooling the planet of Earth [41].

The heat loss from the Earth's surface is greater than the heat from the Sun. If the core does not continue to release heat, the Earth would have cooled off and become a dead rocky globe, like Mars or the Moon. Releasing heat as we know is by nuclear energy from the much slower decays of radioactive elements gradually, such as ^{238}U, ^{235}U, ^{232}Th, and ^{40}K [42]. However, radiogenic heating generated in the core turns iron into a convecting geo-dynamo that maintains a strong magnetic field that shields the planet from the solar wind. This heat leaks out of the core into the mantle, causing convection in the rock that moves crustal plates and fuel volcanoes.

In 1997, it became possible to use seismic tomography to image submerging tectonic slabs penetrating from the surface all the way to the core-mantle boundary [43]. Hotspot's power volcanic activity that continues to produce basalt lava, which forms the Hawaiian Islands and Iceland. Norwegian scientists discovered that basalt eruptions in the Hawaiian Islands and Iceland varied significantly over time [44]. As these two hotspots are located on opposite sides of the Earth, Mjelde, Wessel, and Müller suggested that the co-pulsations represent a global hotspot phenomenon that appears to represent changes in heat from the Earth's core [45]. In 1991, Knittle and Jeanloz suggested that a significant amount of the energy driving the mantle convection is generated in the core [46]. When checking the temperature of the Earth interior, the hottest point is the center of Earth at approximately 7000°C [47], in the inner-core boundary (ICB) at over 6000°C [48], and in the CMB about 4180 ±150°K [49] (Figure 1).

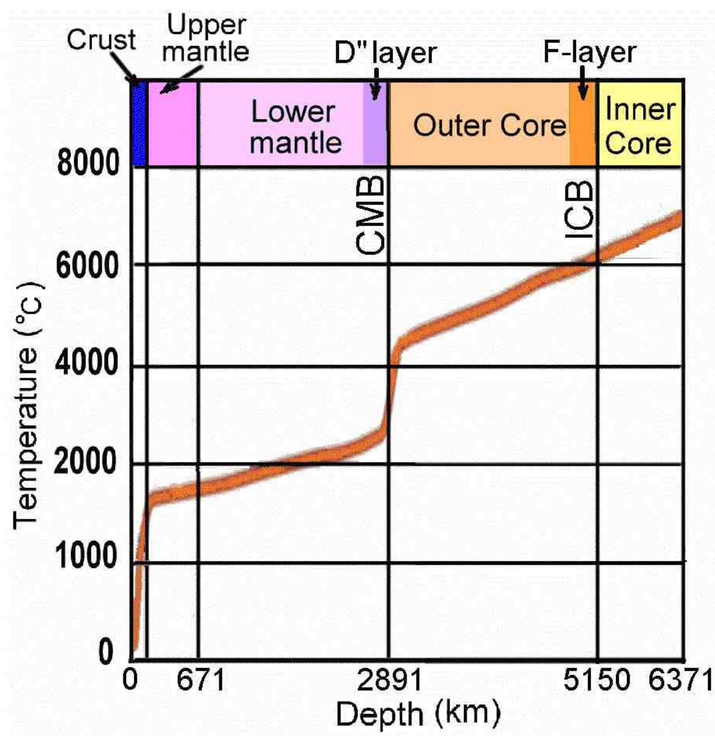

Figure 1. The temperature profile of Earth's interior.

The abundant heat flow from the fluid core leaks out into the mantle. In higher resolution models, the internal effects of the liquid outer core cause some heterogeneities to extend upward from the CMB into the mantle in a manner suggestive of a rising thermal plume structure [50]. Thermal plumes from Earth's core are rising tubes of hot rock that carry more heat away [41].

3.5 Great convection cell spanning the crust through the CMB to the Flayer

On this basis, a large quantity of magma heated at extreme temperatures in the core solidifies into rock, producing the heat of solidification at the CMB. A few quantities of magma absorbing this heat do not solidify but mixes with masses of rock as honeycombed blobs of rock and brings some materials, including magma, osmium-187, ^{3}He, and a little metal, platinum, upward the mantle to pour out at cracks in the mid-ocean ridge to form new ocean floors or in the continent to form great rifts, to disperse the internal heat on the Earth's surface, which works as a secular cooling of the Earth. The downward masses of the slab in the cold regions of the low mantle produce depressions of the CMB into the core, and both the cold region in the mantle and a depression of the CMB produce downwelling flows into the core [36].

The depressed regions of the topography on the CMB are dynamically supported by downwelling of cool mantle materials [37] and then through the CMB into a liquid core, processes that are probably determined by the core. The outer core materials absorb the abundant heat flow and form an upward convection thermal plume.

The energy and buoyancy sources in the core are still not well understood, but we attempt to explain this phenomenon from the perspective of a convection cell. The downward masses of the slab absorb the heat of fusion, diminishing the heat energy at the CMB and melting in the core, where the viscosity is so high that a large quantity of molten rock cannot diffuse but remains as a whole. Thus, the components of molten rock are rarely involved in chemical reactions.

According to mechanics, although the velocity of the downward migrating flow is low, the mass of the slab column from the crust to the CMB is so large that its downward momentum has a great quantity. In the liquid outer core, there is no rigid body with sufficient mass to counteract the downward momentum; thus, the molten rock sinks into the lowermost fluid core. The great downward momentum is counteracted merely by the solid inner core, from which Jeanloz and Wenk obtained possible evidence of low-degree convention like it in the mantle of the inner core from an enigmatic observation [51].

Seismological studies have indicated that the inner core of Earth is anisotropic for *P* waves and has low *S-wave velocity and* high seismic attenuation. The presence of a volume fraction of 3%–10% liquid in the form of oblate spheroidal inclusions aligned in the equatorial plane between iron crystals is sufficient to explain the seismic phenomena. The liquid could arise from the presence a "mushy zone" of dendrites or a mixture of elements other than iron in liquid form under inner-core conditions [52]. Bergman [53] and Shimizu *et al*. [54] suggested that a thin, mushy layer develops underneath the inner-core boundary, while the materials of the outer core solidify onto the inner core. Therefore, the inner core should not be a rigid spheroid. At the ICB, the momentum from the downward molten rock is transmitted through the inner core of the Earth's center, and probably to the opposite side of the CMB. This phenomenon can be inspected using the three-dimensional topographic map of the CMB on Earth (Figure 2) [13].

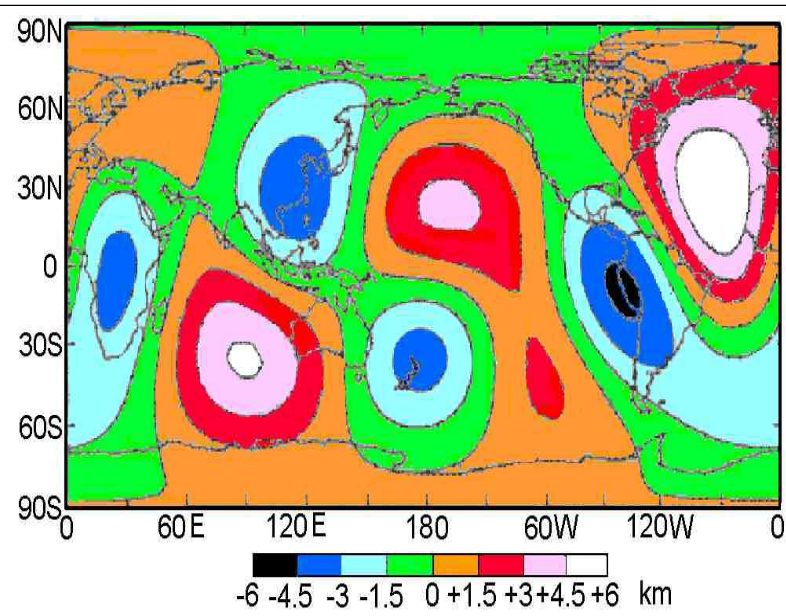

Figure 2. The topography of the CMB obtained by inversion of the combined PcP and PKP_{BC} Data set.

All these it is magma that sinks toward the ICB, and its kinetic energy becomes pressure and spreads into the earth's inner core. It pushes and shoves the opposite side of the ICB, even forming an unsmooth CMB. From the diagram, the CMB is concaving in New Zealand but protruding in the North Atlantic Ocean, and under the west coast of South America, and protruding in the region of Western Australia and near the Indian Ocean, and concaving under South Africa and also protruding in the North Pacific Ocean. There is a significant suggestion that the same materials, dominantly silicates, of the rocky mantle and the liquid outer core change states with each other at the CMB to relieve the CMB topography over 10 km. A reasonable explanation may be that the migrating rock or molten rock of the plate sinks downward, and a magma or thermal plume rises upward in the great convection cell spanning the crust through the F-layer of the outer core.

3.6 Arguments at inner core boundary

The seismic structure of Earth's inner core is highly complex, with strong anisotropy and further regional variations. However, few seismic waves are sensitive to the inner core, and fundamental questions regarding the origin of the observed seismic features remain unanswered [55]. The inner core solidifies from the outer core, but the details of this process remain largely unclear [56].

Seismologists have yet to answer some of the most fundamental questions concerning the core, including the low-velocity gradient region at the lowermost outer core. Numerous seismological studies have suggested that the region just above the ICB is distinct from the rest of the outer core. The layer about 400 km above the ICB was originally termed the F-layer and was characterized by a strong low-velocity zone [57]. After studying the velocity and amplitude in the core, scientists inferred that the highly separated solutions of the F-layer are around the ICB [58-59]. Most observations indicate that the F-layer is global and surrounds the entire inner core [60-63].

From ray theory evidence of a reduced seismic wave velocity gradient to near 0 in the F-layer of the outer core has been interpreted [64-65]. Later Earth models were constructed with more accurate travel-time data but defined as regions of increased velocity. Among the velocity models at the base of the outer core reported by different studies (e.g.: Qamar [59], Dziewonski & Anderson [21], Choy & Cormier [66], Souriau & Poupinet [61], Song & Helmberger [67], Kennett et al. [68] and Yu et al.[69]), the main difference is the structure of the velocity and its gradient at the bottom 400 km of the outer core. According to Earth's models, such as: PREM2 [67], AK135 [68] and Jeffreys-Bullen model [57], Bullen and bolt [70] denote a low-velocity gradient region at the lowermost outer core. In PREM, the velocity increased with a nearly constant gradient around 0.6×10^{-3} s^{-1}. In PREM2 and AK135, the velocity gradient decreases from about 0.6×10^{-3} s^{-1} at 400 km above the ICB to nearly zero at the ICB, and the velocity profile with depth was flatter than that in PREM (Figure 3). Therefore, 400 km above the ICB was chosen as the minimum "pinning depth", at which the models were evaluated and constrained to agree with the PREM in terms of the value and gradient.

While the seismic wave entered the F-layer, a sharp velocity discontinuity appeared at the ICB, the velocity jumped 0.78 km/sec, and a low velocity gradient appeared at the base of the fluid core, indicating slightly different properties of the components. The most robust pointer to the viscosity at the bottom of the outer core may be still the reduced P-velocity gradient, which is difficult to explain without appealing to the existence of a chemical boundary layer [67, 68]. These models imply that near the base of the outer-core density increases too quickly to be explained solely by compression, and that some sort of change in chemistry and phase may occur.

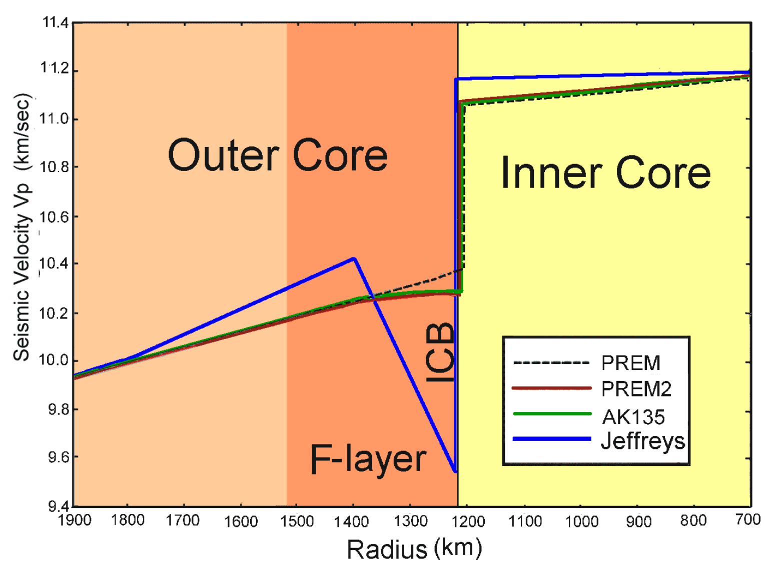

Figure 3. Variation chart of seismic wave velocity in the Flayer: Vp low-velocity gradient and sharp-velocity discontinuity at the ICB indicate their different components.

Experiments [71, 72] and numerical simulations [73] have shown that temperature anomalies generated by strongly heterogeneous CMB heat flux can be transmitted from the CMB to the ICB via outer-core convection. As the Earth cooled and dissipated its internal heat toward the surface through mantle convection, the geographical coincidence of the ICB and CMB anomalies may suggest strong thermal coupling of the mantle and the core, indicating a convection cell across the CMB. The F-layer should have some functions instead of the well-known D" layer, such as thermal and chemical equilibrium.

3.7 Scientists suggested density jumps at the ICB

Regional differences in *PKIKP-PKiKP* travel times and *amplitude* ratio data may originate from the F-layer.Bolt and Qamar [74] first proposed the amplitude ratio (*PKiKP/PcP*) technique and estimated a maximum density jump of 1.8 g/cm^3 at the ICB. Bolt [58] clearly observed both low angle and steep incident reflection of PKiKP of about one second period at the ICB. The mean amplitude ratio *PKiKP/PcP* suggests a density jump Δρ of 1.4 g/cm^3. Souriau and Souriau used the amplitude ratio *PKiKP/PcP* at short distances to constrain the density jump at the inner core boundary to be in the range of 1.35～1.66 g/cm^3 based on array data [75]. Shearer and Masters used "non-observations" of *PKiKP* on the observed amplitude of this phase, leading to upper bounds Δρ=1.8 g/cm^3 at the inner core boundary on the corresponding *PKiKP/PcP* amplitude ratios [76]. Studies have used *PKiKP* to calculate the density jump Δρ across the inner core boundary, and this has remained a topic of debate until now [77]. At the ICB, a density jump of 0.68 g/cm^{3}in the PREM was too small to compare with previous data.

As stated previously, the difference in density between the outer and inner cores must be substantial. Jeanloz and Ahrens [78] conducted shock wave experiments, in which they found that the density of FeO was 10.14 g/cm^3 when reduced to the core temperature and 250 GPA pressure, and under the same conditions, the density of Fe was 12.62 g/cm^3 [79] when FeO became Fe. The difference between the two is 2.48 g/cm^3, which is higher than all other evaluated values.

From this information other than the PREM, the density jump between the lighter liquid outer core and the solid inner core seems to be too large to represent a simple volume change during condensing as the same major components change from a liquid state Fe to a solid state Fe. The composition of the outer core is not likely to be the same as that of the inner core because a liquid in equilibrium with a solid phase in a multi-component system does not have the same composition as a solid [80]. We inferred that the major component of the outer core was mineral silicates, but iron was present in the solid inner core.

On the basis of the free oscillation periods, Derr inferred an earth model ＤI-11 by least-squares inversion with an average shear velocity of 2.18 km/sec in the inner core and a jump in density of 2.0 g/cm^3 at its boundary that satisfied the known mass and moment of inertia [81]. We used the largest density jump of 2.0 g/cm^3 suggested by Derr et al. in this paper to research the new earth model.

3.8 Examining the chemical composition of the core

In order to confirm the favorable constitution of the Earth, the chemical composition of its core must be further investigated. The composition of the Earth's core is one of the most important and elusive mysteries in geophysics. There is no perfect explanation for the chemical equilibrium between the core and the mantle, and the inner core is not in thermodynamic equilibrium with the outer core [14].

The physical and chemical properties of the lower mantle are poorly understood, and the understanding of the coupling mechanisms between the mantle and the core is poor at all timescales. However, the CMB sets boundary conditions for processes occurring within the core, a well-known fact. The topography and lateral temperature variations in the lowermost mantle may have an indistinguishable effect on the magnetic field [82]. Secular variations with periods shorter than a million years but longer than several years almost certainly originate from processes operating in the outer core; unfortunately, there is not yet consensus as to what those processes are [83].

In three-dimensional maps, topographic models represent instantaneous, low-resolution images of a convicting system. Detailed knowledge of mineral and rock properties that are poorly understood at presents required. A complex set of constraints on the possible modes of convection in the Earth's interior that have not yet been worked out; this will require numerical modeling of convection in three dimensions. Thus, the interpretation of the geographical information from seismology data in terms of geodynamic processes is a matter of considerable complexity. The topography of the CMB can be sustained only by dynamic processes, and these processes must be critically understood [84].

The fine structure of the CMB is not well known, but it contains information that is important to geodynamic processes in the mantle, or the magnetic fields generated in the outer core [85]. Approaching the problem of the CMB, Creager and Jordan studied the travel time anomalies of *PKiKP* and PKP_{AB} and corrected the mantle structure in a region in the vicinity of the CMB. They considered some hypotheses regarding the source of anomalies that are the perturbations in the CMB topography. Based on the great convection cell, a relief of the core more than 10 km, as provided by the three-dimensional maps, may be accepted.

As stated previously, the main components of the outer core were similar to those of the lower mantle, i.e., mineral silicates. Based on mineralogy, the main mineral of the mantle is pyrolite, a silicate-containing compound, and the main components of the outer core are also pyrolite but only in liquid form. Under the same conditions, the higher the temperature at which common minerals are produced, the lower is the polymerization rate, and vice versa. The closer the crystal minerals of the mantle were exposed to temperature and pressure, the more the polymerization losses of the crystalline minerals. The bonding forces of the mineral compounds are then destroyed, and crystallization gradually diminishes.

In the F-layer of the deeper core, the high temperature more than 6000°C [48], polymerization may cease completely, and the bonding power of ions mostly loses, and only the electronic bonding force exists. All the ions and molecules may become unbounded. Therefore, the molten rock or magma becomes a mixture of oxides such as FeO, MgO, NiO, SiO_2, Fe_2O_3, Al_2O_3, Cr_2O_3, etc., and metals such as Fe, Ni, and Mn.

According to the temperature profile of the Earth's interior, the center of Earth is made of high-temperature material, which is the hottest point, estimated to be 7000°C [47], which is hotter than the surface of the Sun. In the F-layer, the chemical components may reduce the viscosity; the full fluid oxides and metals can flow, diffuse, float, or sink more freely according to their specific gravity. Estimation of Fe melting temperature at the ICB pressure based on static compression data spans the range 6230 ± 500°K[85].The F-layer above the ICB, in which Fe likes snowflakes falling in the inner core [86].

There are a large amount of iron oxides (FeO, Fe_2O_3) in the mantle, and the deeper the mantle, the higher the proportion of iron oxides. An iron oxide with a metal-like density and electrical properties at high pressure and temperature exists in the Earth's core and may be a compromise between extreme views of the metallic phase and inconformity with the high cosmic abundance of oxygen [87]. From this information, the outer core is rich in iron oxides are proposed.

In view of the topography, the downward migrating magma rich in iron oxides was affected by diffusion, obstruction of the inner core, tangential geostrophic flow, and toroidal flow. Thus, the fluid flowed westward, which may have caused geomagnetic secular variation. Under low viscosity, the oxides and metals can flow easily vertically and horizontally, allowing mutual oxidation-reduction reactions to take place in the F-layer. The active light metals take oxygen from the heavy metal oxides and are further oxidized into light metal oxides, whereas the heavy metal oxides are reduced to heavy metals and precipitate in the inner core. For example:

$$Ca + FeO \longrightarrow CaO + Fe \downarrow$$

$$3Mg + Fe_2O_3 \longrightarrow 3MgO + 2Fe\downarrow$$

$2Al + Fe_2O_3 \longrightarrow Al_2O_3 + 2Fe \downarrow$

$2Cr + 3FeO \longrightarrow Cr_2O_3 + 3Fe \downarrow$

$Mn + NiO \longrightarrow MnO + Ni \downarrow$

CaO, MgO, Al_2O_3, Cr_2O_3, and MnO float in the F-layer, and Fe_2O_3, FeO, and NiO become Fe and Ni, respectively, sinking down to be the main components of the inner core. These oxidation-reduction reactions are exothermic processes that produce large amounts of heat. Reduced iron alloys with certain amounts of Ni settle at the ICB. By far the most provocative mechanism, the F-layer should be maintained through the interaction of the separated melting and solidifying regions distributed over the ICB [88]. In the F-layer, magma diffuses and absorbs a large amount of heat to rise to the CMB, where it condenses into solid rock as the beginning of the process of a large convection cell starts anew.

The great amount of heat produced from radioactive elements generated nuclear energy, chemical reaction heat in the F-layer, and nuclear fission heat near the center of the Earth became the power sources for the geo-dynamo of great convection cells (Figure 4). Therefore, the Earth's geomagnetic secular variations and geodynamic processes operate from the F-layer of the outer core.

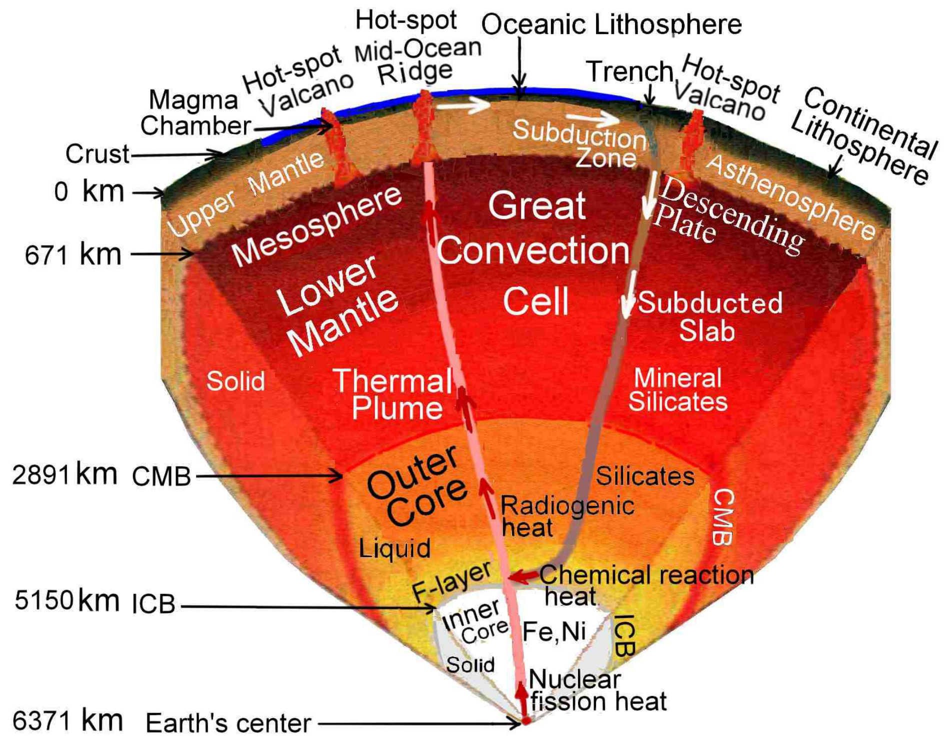

Figure 4. Schematic diagram of the great convection cell, heat flow, and the composition of Earth's interior.

4. Mathematical formulation

4.1 Digital evaluation of data in new earth model

In order to calculate the Earth data, the density distribution follows the divisions of the PREM into 94 levels, including 82 thin shells. The thickness of each shell is not greater than 100 km and so small compared with the Earth's radius of 6371 km that the density is linear variation within it. Then, a simplified method is applied to calculate the information of the Earth in order to simplify the calculation. The formula for the mass M of a uniform sphere can be derived as $M = (4/3)\pi\rho R^3$. The mass ΔM of each shell in the Earth's interior can be calculated as

$$\Delta M = (4/3)\pi\rho_t R_t^3 - (4/3)\pi\rho_b R_b^3 \qquad (1)$$

Where: ρ_t, ρ_b are the densities at the top and bottom, respectively, of a single shell, and R_t and R_b are the radii of the top and bottom in a shell. Because the difference between R_t and R_b is small and the density is regarded as linear variation in the shell, the mean value $\bar{\rho}$ of both ρ_t and ρ_b is substituted for ρ_t and ρ_b in order to simplify the calculation. Then equation (1) becomes

$$\Delta M = (4/3)\pi\bar{\rho}(R_t^3 - R_b^3) \qquad (2)$$

The moment of inertia ΔI of each shell in the Earth's interior can be calculated as

$\Delta I = (8/15)\pi\bar{\rho}(R_t^5 - R_b^5)$ (3)

From fluid mechanics, in a region of uniform composition, which is in a state of hydrostatic stress, the gradient of hydrostatic pressure can be expressed as

$dP/dR = -g\rho$ (4)

Here, P and R are the pressure and radius, respectively, in the region; ρ is the density at that depth; g is the acceleration due to gravity at the same depth. If the effect of Earth's rotation is negligible, the potential theory shows that g is resulted only from the attraction of mass M within the sphere of radius R through

$g = GM/R^2$ (5)

Where: G is the gravitational constant ($6.6726\times10^{-11} m^3/kg.s^2$). Equation (5) substitutes into equation (4) and integrates it. In order to simplify the calculation, ρ and M are substituted by $\bar{\rho}$ and $\bar{m}$, which are considered constants in the thin shell and are irrelative to P and R. The result becomes

$\Delta P = (1/R_b - 1/R_t)G\overline{m\rho}$ (6)

Where: ΔP is the difference in pressure between the top and the bottom in a layer of the Earth, and $\bar{m}$ is the mass of a sphere as the mean value of the masses of the sphere within the top radius R_t and the bottom radius R_b, respectively, of a shell. Equation (6) cannot be applied to the center of Earth, where is a discontinuous point. To integrate the portion of the center, the other form is applied as follows:

$\Delta Pc = (2/3)\pi G\bar{\rho}^2 R_c^2$ (7)

Where: Δ Pc is the difference in pressure between the radius R_c and the center of the Earth at the center. The acceleration due to gravity g of each layer can be derived from equation (5). According to the observation data, the moment of inertia for the polar axis of the earth is $0.3309 MeRe^2$ and about an equatorial axis is $0.3298 MeRe^2$ [130]. The earth is regarded as a sphere, of which the moment of inertia is determined to be 80286.4×10^{40} $g.cm^2$ by taking the mean value of both figures, where Me is the earth's mass of 5974.2×10^{24} g and Re is the equatorial radius of 6378.14 km.

To examine the accuracy of the applied equations, we applied the density distribution of the PREM to calculate the Earth's mass, moment of inertia, pressure, and gravitational acceleration. The calculated values of the earth's data from the density distribution of the PREM as compared with the values of the current data and the PREM are listed in compared with that of the current data and the PREM are listed in Table 1 (http://newidea.org.tw/pdf/S60.pdf) and Table 2.

Table 2. Calculated values from the density distribution of the Earth compared with the data, PREM, and current Earth.

Data of the Earth	Mass	Moment of inertia	Pressure at the CMB	Pressure at Earth's center	Gravity at the CMB	Gravity at Earth's surface
Unit	10^{24} g	$10^{40} g.cm^2$	K bar	K bar	cm/sec^2	cm/sec^2
PREM and Current	5974.200	80286.400	1357.509	3638.524	1068.230	981.560
Calculated values	5973.289	80205.664	1358.335	3655.973	1068.680	981.959
Difference %	-0.0152	-0.1006	+0.0608	+0.4796	+0.0421	+0.0406

From Table 2, the deviations of the calculated Earth's values from the PREM data and the current Earth are nearly within 0.1%, except for the pressure at the Earth's center. This indicates that the calculated values are very close to the current data and that the simplified method is acceptable and useful; however, the calculated pressure of 3655.973 kbar at the Earth's center is higher than the data of the PREM of 3638.524 kbar by 0.4796 %, about 8 times of deviation at the CMB. We compared all calculated pressures of the simplified method with that of the PREM using the curve of deviation E in Table 3 (http://newidea.org.tw/pdf/S61.pdf) and show the pressure P of the PREM in Figure 5.

.

According to Figure 6, the deviation E of the pressure curve from the crust to the CMB is nearly a straight line, indicating that the calculated pressures have systematic errors from the error theory. However, from the CMB to the Earth's center, the slope of curve E increases sharply above the dashed line, which is the straight line extended from the CMB. This indicates that there is considerable discrepancy in the core. We may suppose that the structure of the PREM core, which greatly affects its core pressure, is flawed.

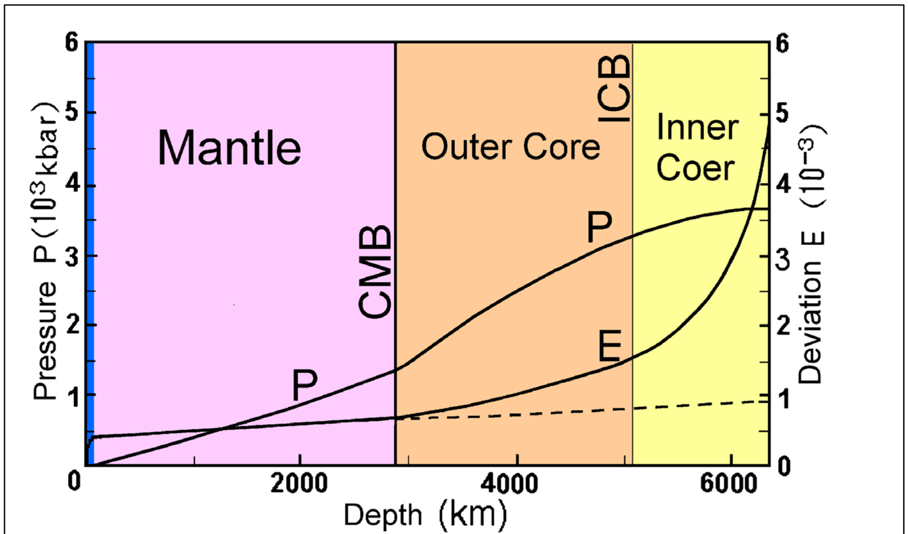

Figure 5. Pressure P of the PREM and deviation E of the calculated pressure using the simplified method from the value of P

In order to investigate the structure of the Earth, particularly the core, four curves of density distribution are proposed to match the known conditions. From the crust to the CMB the curves of density distribution are adopted as the PREM, and from the CMB to the ICB, four different plotted curves were assumed. Due to a small jump in the P-wave velocity at the boundary of the F-layer in the outer core, the slope of the density curve was nearly as steep as that of the PREM. There is a discontinuity at the ICB, so a density jump of Derr's suggestion (2.0 g/cm^3) is used [89]. In the inner core, the slope of the density curve of PREM was the same. The four density curves of the assumed Earth model compared with the PREM are shown in Figure 6.

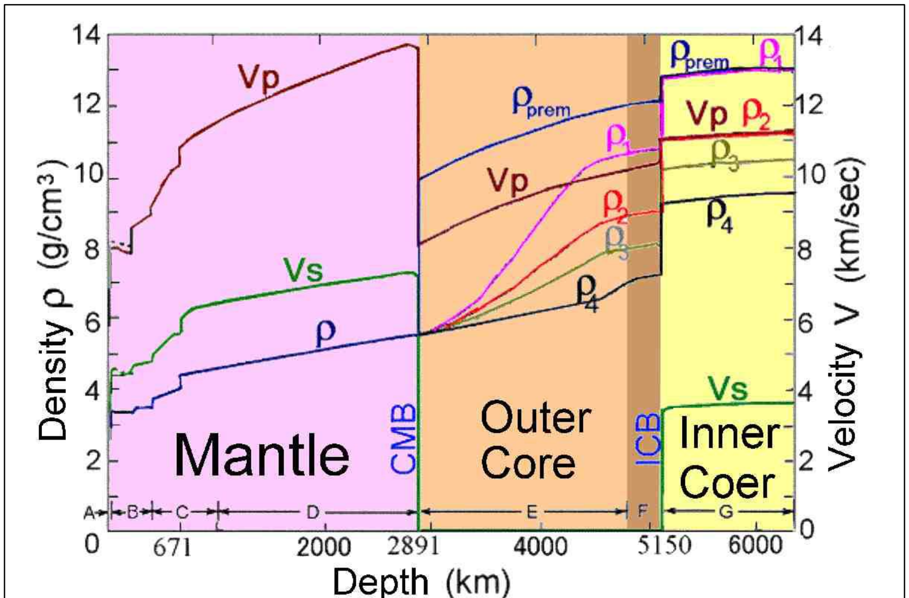

Figure 6. These densities ρ of the new Earth models 1, 2, 3, and 4 were compared with the PREM's.

The mass and moment of inertia of the four new Earth models can be determined and compared with the current measured data of the Earth's mass of 5974.2×10^{24}g and moment of inertia of 80286.4×10^{40} g.cm^2, so the differences will be found to be very large, as shown in Table 4. The differences are the mass insufficiencies and the moment of inertia in the four new Earth models.

Table 4. Insufficiencies of mass and moment of inertia in the four new earth models.

Earth model	Unit	Observed value	New Model 1.	New Model 2:	New Model 3.	New Model 4:
Mass	10^{24}g	5974.200	5409.024	5268.126	5204.761	5121.820
Insufficiency	10^{24}g	-	565.176	706.074	769.439	852.380
Moment of inertia	10^{40}g.cm^2	80286.400	77007.472	76571.028	76378.768	76126.841

Insufficiency	10^{40}g.cm^2	-	3278.928	3715.372	3907.632	4159.559

The insufficiency in the Earth's mass and moment of inertia, called the missing mass and moment of inertia, are relative to the gravity of dark matter in astrophysics. It can only be obtained by comparing the observed data of the Earth, which cannot be detected directly and answered clearly through ordinary Earth sciences. To solve the problems of insufficiencies, a new study of the Earth is attempted by using contemporary physics. If we successfully explain that insufficient conditions exist under suitable conditions, a new Earth model will be established.

4.2 Digital evaluation of data in dark planet

Proceeding with this assumption, the missing mass and moment of inertia of Earth are assumed to be those of cold dark matter (CDM), which may constitute a normal planet. In order to find a solution for this paper, dark matter is compared to Mars. The average radius of Mars is 3397 km, and the mass 642.40×10^{24} g. In1989, Kaula *et al.* studied the moment of inertia of Mars and obtained the maximum allowable mean value is 0.3650 MR², i.e., 2689.8×10^{40} g.cm^2 [90]. The insufficient data of 4 new Earth models roughly approach to the Mars", So, the dark matter is considered as a planet, called a dark planet, whose form is similar to Mars, and whose characteristics are based on the inner planets of the solar system. To cut a figure of the dark planet, it is considered a sphere whose radius and density can be calculated from the insufficiencies in the Earth's mass and moment of inertia through the simplified method. The dark planet data can be calculated as following.

Considering the density of rock on the surfaces of the Earth and Moon, a surface density of 2.70 g/cm^{3}of the dark planet is proposed. Under the condition that the density of a layer is proportional to its depth, a trial value of density at the center of the dark planet is selected. Applying equations (2) and (3) to calculate the mass and moment of inertia of each shell, the total mass and moment of inertia of each shell can be obtained. Because the radius and center density of the dark planet are hypothetical values, the total mass and moment of inertia must correspond to the insufficiencies of the Earth's mass; therefore, it is necessary to use a trial-and-error approach to determine the proper radius and center density.

Since the Earth's orbit around the Sun may be affected by the gravity of the dark planet, no abnormal effects on the Earth have been observed. It is assumed that the gravity centers of Earth and the dark planet coincide at the same time. It is inferred from the phenomenon in which the same side of the Moon always faces the Earth, meaning that the Earth and the dark planet may rotate synchronously.

Assuming that the gravity centers of the Earth and the dark planet coincide at a single point, and both rotate synchronously, the total mass and moment of inertia may be obtained from. Based on mechanics, the gravity of each shell inside the Earth is affected by the mass of the Earth and the dark planet within its radius. The pressure difference $\Delta P'$ between the top and bottom of a shell in the Earth is calculated through

$$\Delta P' = (1/R_b - 1/R_t) G \overline{M}' \overline{\rho} \quad (8)$$

Where: $\overline{M}'$ is the mean value of the total mass of the Earth and the dark planet within radius R_t and R_b.

Equation (8) cannot be applied to the Earth's center. The average density $\overline{\rho}'$ of the central portion combined with the Earth and the dark planet within radius Rc can be calculated as follows:

$$\overline{\rho}' = (Mc + Md) / [(4/3)\pi Rc^3] \quad (9)$$

Where: Mc and Md are the masses of the central portion on Earth and the dark planet, respectively.

The difference in pressure $\Delta P_c'$ between the top and center of the central portion of Earth can be obtained as

$$\Delta P_c' = (2/3)\pi G \overline{\rho} \overline{\rho}' Rc^2 \quad (10)$$

Based on the characteristics of the inner planets of the solar system except for Mercury, a planet with a larger radius has a higher average density. Therefore, the radius and average density of a suitable dark planet must be compatible with the characteristics of the inner planet in the solar system. The data of the four new Earth models and each dark planet were compared with the data of the current Earth and the PREM (Table 5).

Table 5: Calculated data of the four new earth models compared with the data of the current earth and the PREM

Kind of Earth's model	The Earth planet							The dark planet					Suitability
	Radius	Average density	Mass	Moment of inertia	Center density	Center pressure	Moment of inertia	Radius	Average density	Mass	Moment of inertia	Moment of inertia	
Unit	km	g/cm3	10^{24}g	10^{40} g.cm^2	g/cm^3	kbar	C	km	g/cm^3	10^{24}g	10^{40} g.cm^2	C	
PREM	6371	5.5150	5974.200	80286.400	13.08848	3638.524	0.3309						
Model1	6371	4.9945	5409.024	77007.472	13.08848	3283.754	0.3508	3808.414	2.4427	565.176	3278.928	0.4000	no
Model2	6371	4.8635	5268.126	76571.028	11.29785	3039.584	0.3581	3732.304	3.2421	706.074	3715.372	0.3777	no
Model3	6371	4.8050	5204.761	76378.768	10.46002	2934.587	0.3615	3717.755	3.5747	769.439	3907.632	0.3674	no
Model4	6371	4.7284	5121.820	76126.841	9.49821	2805.297	0.3662	3700.375	4.0161	852.380	4159.559	0.3564	good

The average radius of Mars is 3397 km, the mass 642.40×10^{24} g, and its average density is 3.912 g/cm^3.Both values of the radius and the average density of the dark planet in the new Earth model 4 are larger than those of Mars; therefore, this model is found to be the more suitable one.

The precise data for the Earth and the dark planet were calculated from the density distribution of the new Earth model 4. The data for the Earth planet are listed in Tables 6 (http://newidea.org.tw/pdf/S62.pdf), the dark planet is listed in Table 7 (http://newidea.org.tw/pdf/S63.pdf), and the global data for the new Earth model in Table 8 (http://newidea.org.tw/pdf/S64.pdf). The pressure P and the acceleration due to gravity g of the new Earth model compared with the PREM are shown in Figure 7. In this suitable model, the slope of the density curve from a depth of about 400 km of the upper mantle through zones C, D, and E to the upper boundary of the F-layer is nearly a straight line, which means that the density increases in proportion to its depth in accordance with general physical phenomena. Therefore, the new Earth model 4 is considered the proper new Earth model. We find that the pressure curve of the new Earth model is smoother than that of the PREM below the CMB. In the gravity curve of the new Earth model, there are two deflection points in the curve: one is at 2670.625 km deep at the radius of the dark planet, and the other is at the ICB. The Earth has a mass of 5121.820×10^{24}g, a moment of inertia of 76126.841×10^{40} g.cm^2, and an average density of 4.7284 g/cm^3. The Earth's center has a density of 9.49821 g/cm^{3}and the pressure of 2805.297 kbar. The reduced values of the Earth's data relative to the current Earth are due to the existence of the dark planet. The dark planet has a radius of 3700.375 km, a moment

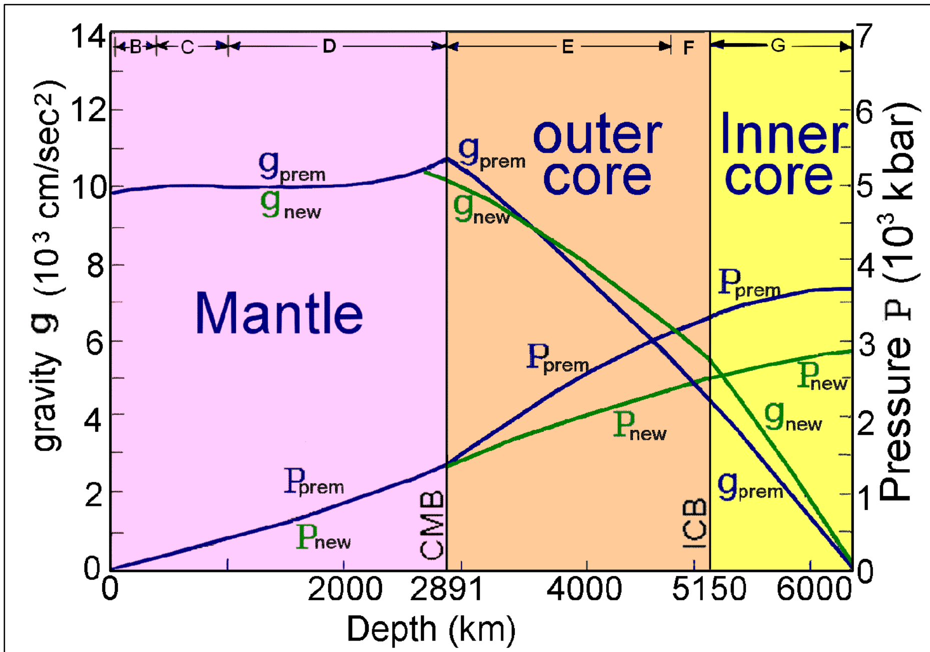

Figure 7. Diagram of the gravity g and the pressure P of the new Earth model and the PREM.

of inertia of 4159.559×10^{40}g.cm^2, an average density of 4.0161 g/cm^{3}and a mass of 852.380×10^{24}g about 1.33 times that of Mars. The data for the new Earth model compared with those of the current Earth and the PREM are listed in Table 8.

Table 8. The data of the new earth model are compared with those of the current earth and the PREM.

Data of planet	**Radius**	**Mass**	**Inertia of moment**	**Average density**	**Center density**	**Center pressure**	**Coef-ficient**
Unit	km	10^{24}g	10^{40} g.cm^2	g/cm^3	g/cm^3	kbar	C
PREM and current earth	6371.000	5974.200	80286.400	5.515	13.08848	3638.524	0.3309
Earth planet	6371.000	5121.820	76126.841	4.7284	9.49821	2805.297	0.3662
Dark planet	3700.375	852.380	4159.559	4.0161	7.96097	1115.272	0.3564

The density of the Earth's center was 9.49821 g/cm^3, which is much lower than the density of 13.08848 g/cm^{3}of the PREM. The pressure was 2805.297 kbar, which is much lower than the 3638.524 kbar of the PREM. The composition of the inner core is generally believed to be predominantly Fe with a small amount of alloyed Ni. From the pressure- density Hugoniot data, the density of iron under 2805.297 kbar of pressure is about 12.7 g/cm^3[91], which is much greater than that of the new Earth model by 25%. The inner core is not pure iron but contains a significant fraction of light components [92, 93], which explains why the density of the inner core is much smaller than the current value. Therefore, an inference that the composition of the inner core is predominantly Fe, alloyed with a small amount of Ni, and combined with a significant amount of oxides is suggested.

5. Results and Discussion

From the conceptions of String theory, a new study in a different view of the core developed a new Earth model, in which the great convection cells of magma and solid or molten rock migrate up to the crust and down across the CMB to the lowermost F-layer of the outer core, causing the more than 10 km relief of the CMB, and from the core brings some matter as the metal platinum has come all the way to the surface of the Earth.

This study introduces a new Earth model that should solve some inexplicable problems in Earth science, such as the density jump, the core-mantle chemical equilibrium, geomagnetic secular variation and the Chandler wobble, and the anomalous properties of the CMB and the ICB should also be brightened.

From the simplified method of evaluating the data of the new Earth model compared with the current observed data of the Earth, there are 14.27% of the mass and 5.18% of the moment of inertia missing, which evaluates a dark planet inside the Earth from the conceptions of String theory.

From the 10-dimensional space-time of String theory, the 3-cosmic framework of the universe was developed, i.e., multiverse, and triple cosmoses existed in the whole space, namely 1st cosmos, 2nd cosmos and 3rd cosmos. According to String theory, there is no relationship between any two cosmoses except for gravitational force, which is a characteristic of dark matter. This study may serve as an indirect proof of the existence of dark matter, which is located in the interior of the Earth but other cosmos than ours.

It is difficult to directly examine the existence of dark matter; however, this can be recognized from Chandler's wobble. Referring to the orientation of the rotation axis of the Earth in space in addition to both precession and nutation, there is a wobble on the instantaneous axis of rotation of the Earth. The wobble alters the position of a point on the Earth relative to the pole of rotation. In 1891, Chandler pointed out that there are two distinct kinds of the wobble periods. The first is a period of 12 months, and the second is a period of 433 days, which is approximately 14 months. The former, called annual wobble, is obviously affected by the seasonal climate. The latter, called Chandler wobble, has not been solved for more than one hundred years [94]. The Chandler wobble is a small deviation that changes by approximately nine meters at the point on the surface of the rotation axis of the Earth.

In 2000, Gross found that two-thirds of the Chandler wobble was caused by fluctuating pressure on the seabed, which, in turn, is caused by changes in the circulation of the oceans caused by variations in temperature, salinity, and wind. The remaining third is due to atmospheric fluctuations [95]. The full explanation of this period also involves the fluid nature of the Earth's core and oceans. The wobble, in fact, produces a negligible ocean tide with an amplitude of approximately 6 mm, called a "pole tide", which is the only tide not caused by an extraterrestrial body. While it has to be maintained by changes in the mass distribution or angular momentum of the Earth's outer core, atmosphere, oceans, or crust (from earthquakes), for a long time the actual source was unclear because no available motions seemed to be coherent with what was driving the wobble.

It is inferred from the phenomenon in which the same side of the Moon always faces the Earth, meaning that the Moon and Earth rotate synchronously. The same phenomenon will happen to the Earth and the dark planet in which both rotate synchronously, but the rotation axes of both are impossible to coincide with each other, i.e., an angle between the two rotation axes produces the Chandler wobble as the precession and nutation due to the effects of the Sun and Moon on non-parallel rotation axes with the Earth's. Therefore, the effect of Chandler wobble may confirm the existence of a dark planet inside the Earth but in other cosmos than ours.

From this study, the hypothesis of the three-cosmic framework of the universe may enable a new way to discover abundant dark matter and solve some problems in astrophysics, such as the following:

1. Cygnus X-1 is a hot supergiant star orbited by an invisible compact object with a period of 5.6 days [96]. The mass of a compact object can be estimated from Doppler shifts in the spectrum of a visible supergiant star. Its mass is about 9 times of the sun. This is considerably greater than the maximum mass of a neutron star. Therefore, the compact object is not a neutron star nor a white dwarf star. Because there are optical confirmation problems, the compact object may not be a black hole. If we consider the compact object of Cygnus X-1 as dark matter in a cosmos other than ours, and its gravity affects Cygnus X-1, the problem may be solved.
2. Stars that evaporate from the Hyades cluster will remain within a few hundred parsecs (1 parsec =3.26 light year; pc) of the cluster only if they are dynamically bound to a much more massive entity containing the cluster. A local mass enhancement of at least $(5\sim10)\times10^5$ solar masses with a radius of about 100 pc can trap stars with an origin related to that of the Hyades cluster and explains the excess of stars with velocities near the Hyades velocity that constitutes the Hyades supercluster. Part of this mass enhancement can occur in visible stars, but a substantial fraction is likely to occur in the form of dark matter [97]. This dark matter should exist in other cosmos than ours.
3. Historically, the prediction of Halley's Comet bas always involved errors of 3 or 4 days in the predicted time of the perihelion passage. Joseph Brady, a scientist at the California Institute of Technology, based on studies of periods of Halley's Comet using old European and Chinese records and using a computer to treat the data of it in a numerical model of the solar system, he was able to predict an invisible X planet (trans-plutonian planet), which was about three times the size of Saturn with a highly inclined orbit (i=120°, e= ± 0.07) to the ecliptic and the time period of it to be 450 years [98, 99]. Flandern proposed a search for an X planet, which has approximately three times the mass of Earth and a highly inclined eccentric orbit that accounts for all the perturbations in the motions of Neptune [100]. In 1988, NASA research scientist Anderson presented the deviation of Neptune and Uranus in the regular orbit and proposed "The Theory of X Planet" based on observed astronomical data from the 19th century. The mass of planet X is approximately five times that of the Earth, and its period is about 700～1000 years. The orbit is elliptical, and the inclination from the orbit to the ecliptics is very large and almost perpendicular [101]. Planet X has been searched for, but it remains to be found. If dark planet X orbits around the Sun in a universe other than ours, its gravity may sometimes affect the motions of

Halley's Comet, Neptune, and Uranus. Therefore, the problem of invisible planet X can be solved.
This is an absolute new attempt to break the bottlenecks of research on the deep interior of the Earth in geophysics and in the spaces of the universe in astrophysics. From the applications of the ten-dimensional space-time of String theory, a three-cosmic framework of the universes is inferred. Some scientific problems in geophysics and astrophysics may be roughly solved, but they still need to be proved by the fine outcomes of physicist research.

References

[1]. Zwicky, F. (1937). On the Masses of Nebulae and of Clusters of Nebula. *Astrophysical Journal*, 86: 217.
[2]. Bartusiak, M. (1988). Wanted: Dark Matter, *Discover*, Dec., 63-69.
[3]. Stsrobinskii A. A. & Zel'dovich, Z. B. (1988). Quantum Effects in Cosmology, *Nature,* 331: 25.
[4]. Riess Adam G. *et al*. (High-z Supernova Search Team) (1998). Observational Evidence from Supernovae for an Accelerating Universe and a Cosmological Constant. *Astronomical J.* 116 (3): 1009-1038.
[5]. Perlmutter, S.; Aldering; Goldhaber; Knop; Nugent; Castro; Deustua; Fabbro; Goobar; Groom; Hook; Kim; Kim; Lee; Nunes; Pain; Pennypacker; Quimby; Lidman; Ellis; Irwin; McMahon; Ruiz-Lapuente; Walton; Schaefer; Boyle; Filippenko; Matheson; Fruchter; et al. (1999). Measurements of Omega and Lambda from 42 High-Redshift Supernovae. *Astrophysical Journal,* 517 (2): 565-586.
[6] Planck Collaboration: Aghanim, N. et al. (2020). Planck 2018 results. VI. Cosmological parameters. Astronomy & Astrophysics, 641(A6): 7, Table 1. Base-ΛCDM cosmological parameters from Planck TT, TE, EE + lowE + lensing, Plik best fit.
[7]. Scherk, J. & Schwarz, J. H. (1975). Dual field theory of quarks and gluons, *Physics Letters*, B, 57:463- 466.
[8]. Siegfried, T. (1999). Hidden Space Dimensions May Permit Parallel Universes, Explain Cosmic Mysteries. *The Dallas Morning News*, 5 July.
[9]. Dvali, G. (2004). Out of the Darkness, Scientific American, February, 68-75.
[10]. Guth, A. H. (1982). Fluctuation in the New inflationary, Physical Review Letters, 49 (15): 1110–1113.
[11]. Everett, Hugh, (1957). Relative State Formulation of Quantum Mechanics. *Reviews of Modern Physics.* 29: 454-462.
[12]. Byrne, P. (2008). The Many Worlds of Hugh Everett**,** *Scientific American*, on October 21.
[13]. Creager, K. C. & Jorden, T.H. (1986). A spherical structure of the core-mantle boundary from PKP travel time, *Geophysics. Res. Lett*., 13: 1497-1500.
[13]. Morelli, A. & Dziewonski, M. (1987). Topography of the core-mantle boundary and lateral homogeneity of the liquid core, *Nature*, 19, Feb., 325: 678-683.
[14]. Jeanloz, R. (1990). The Nature of the Earth's Core, *Annual Review of Earth and Planetary Sciences,* 18: 357-386.
[15]. Dziewonski, A.M. & Anderson, D. L. (1981). Preliminary Reference Earth Model, *Phsy. Earth Planet, Inter.*, 25, 297-356.
[16]. Ramsey, W. H. (1948). On the constitution of the terrestrial planets, *Mon. Not. Roy. Astron. Soc.*, 108: 406-413.
[17]. Lyttleton, R.A. (1973). The end of the iron-core age, *Moon*, 7: 422-439. [24].
[18]. Knopoff, F. (1965). A preeminent seismology, Phys. Rev., 138 (A): 1445.
[19]. Buchbinder, G. G. R. (1968). Properties of the Core-Mantle Boundary and Observations of PcP, *J. Geophys. Res*., 73: 5901.
[20]. Agnew, D., Berger, J., Buland, R., Farrell w. & Gilbert, F. (1976). International Deployment of Accelerometers: a network for very long period seismology, *EOS, Trans. Am. Geophys. Union*, 57: 180-188.

[21]. Peterson, J., Butler, H. M., Holcomb, L. G. & Hutt, C. R. (1976). Seismic research observatory, *Bull. Seism. Soc. Am*. 66: 2049-2068.

[22]. Doornbos, D.J. & Hilton, T. (1989). Models of the core-mantle boundary and the travel times of internally reflected core phases, *J. Geophys. Res.*, 94 (B11): 15,741-15,751.

[23]. Forte, A. M. & Peltier, R. W. (1991). Mantle convection and core-mantle boundary topography: Explanations and implications, *Tectonophysics*, 187 (1-3): 91-116.

[24]. Neuberg, J. & Wahr, J. (1991). Detailed investigation of a spot on the core mantle boundary using digital PcP data, *Phys. Earth planet. Inter.*, 68: 132-143.

[25]. Rodgers, A. & Wahr, J. (1993). Inference of core-mantle boundary topography from ISC PcP and PKP travel times. *Geophys. J. Int.* 115: 991-1011.

[26]. Obayashi, M. & Fukao, Y. (1997). P and PcP travel time tomography for the core-mantle Boundary. *J. Geophys. Res.*, 102: 17825-17841.

[27]. Boschi, L. & Dziewonski, A. M. (1999). High- and low- resolution images of the Earth's mantle: Implications of different approaches to tomographic modeling, *J. Geophys. Res.*, 104 (B11): 25567- 25594.

[28]. Boschi, L. & Dziewonski, A. M. (2000). Whole Earth tomography from delay times of P, PcP, and PKP phases lateral heterogeneities in the outer core or radial anisotropy in the mantle? *J. Geophys. Res.*, 105: 13675-13696.

[29]. Garcia, R. & Souriau, A. (2000). Amplitude of the core-mantle boundary topography estimated by stochastic analysis of core phases. *Phys. Earth Planet. Inter.*, 117: 345-359.

[30]. Sze, E.K.M. & van der Hilst, R. D. (2003). Core Mantle Boundary Topography from Short Period PcP, PKP and PKKP data, *Physics of the Earth and Planetary Interiors*, 135: 27-46.

[31]. Yoshida, M. (2008). Core-mantle boundary topography estimated from numerical simulations of instantaneous flow. *Geochem. Geophys. Geosys*. 9 (7).

[32]. Soldati, G., Koelemeijer, P., Boschi, L. & Deuss, A. (2013). Constraints on core-mantle boundary topography from normal mode splitting: *Geochem. Geophys. Geosyst*. 14.

[33]. Soldati, G., Boschi, L., Mora, S. D. & Forte, A. M. (2014). Tomography of core-mantle boundary and lowermost mantle coupled by geodynamics: joint models of shear and compressional velocity, *Annals of Geophysics,* 6: 57.

[34]. Young, C. J. & Lay, T. (1987). The core-mantle boundary, Ann. Rev. Earth Planet. Sci., 15: 25-46.

[35]. Ruff, L. Anderson, D. L. (1980). Core formation, evolution, and convection: A geophysical model, *Phys. Earth Planet. Inter.*, 21**:** 181-201.

[36]. Bloxham, J. & Jackson, A. (1990). Lateral temperature variations at the core-mantle boundary deduced from the magnetic field, *Physical Review Letters*, 17 (11): 1997-2000.

[37]. Lay, T. (1989). Structure of the Core-Mantle Transition Zone: A Chemical and Thermal Boundary Layer, *EOS*, Jan., 70(4): 24, 49, 54-55, 58-59.

[38]. Gubbins, D. & Richards, M. A. (1986). Coupling of the core dynamo and mantle: Thermal or Topography? *Physical Review Letters*, 13: 1521-1524.

[39]. Morgan, W.J. (1971). Convection plumes in the lower mantle: *Nature*, 230: 42-43.

[40]. Morgan, W.J. (1972). Deep mantle convection plumes and plate motions, *Bull. Am. Assoc. Pet. Geol.*, 56: 203-213.

[41]. Hand, E. (2015). Mantle plumes seen rising from Earth's core, *Science*, 349 (6252): 1032-1033.

[42]. Van Schmus, W. R. (1995). Natural radioactivity of the crust and mantle, *Global Earth Physics: A Handbook of Physical Constants*, 283-291.

[43]. Kerr, R. A. (1997). Deep-Sinking Slabs Stir the Mantle. *Science.* Retrieved 2013-06-13.

[44]. Mjelde, R. & Faleide, J. I. (2009). Variation of Icelandic and Hawaiian magmatism: evidence for co-pulsation of mantle plumes? *Mar. Geophys. Res.*, 30: 61-72.

[45]. Mjelde, R. Wessel, P. & Müller, D. (2010). Global pulsations of intraplate magmatism through the Cenozoic. *Lithosphere*, 2 (5): 361-376.

[46]. Knittle, E. & Jeanloz, R. (1991). The high-pressure phase diagram of $Fe_{0.94}O$: A possible constituent of the Earth's core, *J. Geophysics Res.*, 96: 16169-16180.

[47]. Kubala, Bizy, & Mahan Rao, (1996). Earth's Core Temperature. *Byrdand Black.*

[48]. Condie, Kent C. (1997). *Plate tectonics and crustal evolution* (4th Ed.). Butterworth-Heinemann, p. 5.

[49]. Fiquet, G., Auzende, A. L., Siebert, J., Corgne, A., Bureau, H., Ozawa, H. & Garbarino, G. (2010). Melting of peridotite to 140 gigapascals. *Science*, 329: 1516-1518.

[50]. Young, C.J. & Lay, T. (1987). The core-mantle boundary, *Ann. Rev. Earth Planet. Sci*., 15: 25-46.

[51]. Jeanloz, R. & Wenk, H. R. (1988). Convection and anisotropy of the inner core, *Geophysics. Res. Lett*. 15: 72-75.

[52]. Singh, S. C., Taylor, M. A. J. & Montagner, J. P. (2000). On the presence of liquid in Earth's inner core. *Science*, 287: 2471-2474.

[53]. Bergman, M. I. (2003). Solidification of the Earth's core, in Earth's Core: Dynamics, Structure, Rotation, *Geodyn. Ser.*, 105-127.

[54]. Shimizu, H., Poirier J. P. & Le Mouël, J. L. (2005). On crystallization at the inner core boundary. *Phys. Earth Planet. Inter*. 151: 37-51.

[55]. Waszek, L. & Deuss, A. (2015a). Observations of exotic inner core waves, *Geophys. J. Int.*, 200 (3): 1636-1650.

[56]. Pejić, T. & Tkalčić, H. (2016). Toward attenuation tomography of the uppermost inner core from PKP waves, *Geophysical Research Abstracts,* 18: EGU 2016-1605.

[57]. Jeffreys, H. (1939). The times of the core waves, *Mon. Not. R. Astron. Soc. Geophys. Suppl*., 4: 498.

[58]. Bolt, Bruce A. (1972). The density distribution near the base of the mantle and near the Earth's center, *Phys. Earth Planet. Inter.*, 5: 301-311.

[59]. Qamar, A. (1973). Revised velocities in the Earth's core, *Bull. Seismol. Soc. Am*., 63: 1073- 1105.

[60]. Cormier, V. F. (2009). A glassy lowermost outer core. *Geophys. J. Int.*, 179: 374-380.

[61]. Souriau, A. & Poupinet, G. (1991). The velocity profile at the base of the liquid core from PKP (BC + Cdiff) data: An argument in favor of radial inhomogeneity, *Geophys. Res. Lett.*, 18: 2023-2026.

[62]. Zou, Z., Koper, K. D. & Cormier, V. F. (2008). The structure of the base of the outer core inferred from seismic waves diffracted around the inner core, *J. Geophys. Res.*, 113: B05314.

[63]. Cormier, V. F., Attanayake, J. & He, K. (2011). Inner core freezing and melting constraints from seismic body waves. *Phys. Earth Planet. Inter*., 188: 163-172.

[64]. Rial, J. A. & Cormier, V. F. (1980). Seismic waves at the Epicenter's antipodes, *J. Geophys. Res.*, 91: 10203-10228.

[65]. Cormier, V. F. (1981). Short-period PKP phases and the inelastic mechanism of the inner core, *Phys. Earth Plant Inter. 24: 291*-301.

[66]. Choy, G. L. & Cormier, V. F. (1983). The structure of the inner core inferred from short-period and broad-band GDSN data, *Geophys. J. R. Astr. Soc.*, 72: 1-21.

[67]. Song, X. & Helmberger, D. V. (1995). A P wave velocity model of earth's core, *J. Geophys. Res.*, 100 (B7): 9817-9830.

[68]. Kennett, B. L. N., Engdahl, E. R. & Buland, R. (1995). Constraints on seismic velocities in the Earth from travel times, *Geophys. J. Int.*, 122: 108- 124.

[69]. Yu, W., Wen, L. & Niu, F. (2005). Seismic velocity structure in the Earth's outer core, *J. Geophys. Res.*, 110: B02302.

[70]. Bullen, K. E. & Bolt, B. A. (1986). *An Introduction to the Theory of Seismology*, 4th Ed., Geophysical Journal of the Royal Astronomy Soc., 86 (1): 215-216.

[71]. Sumita, I. & Olson, P. (1999). A laboratory model for convection in Earth's core driven by a thermally heterogeneous mantle. *Science*, 286: 1547-1549.

[72]. Sumita, I. & Olson, P. (2002). Rotating thermal convection experiments in a hemispherical shell with heterogeneous boundary heat flux: implications for the Earth's core. *J. Geophys. Res.*, 107: 2169.

[73]. Aubert, J., Amit, H., Hulot, G. & Olson, P. (2008). Thermochemical flows couple the Earth's inner core growth to mantle heterogeneity, *Nature*, 454: 758-762.

[74]. Bolt, Bruce A. & Qamar, A. (1970). Upper bound to the density jump at the boundary of the Earth's inner core, *Nature*, 228: 148-150.

[75]. Souriau, A. & Souriau, M. (1989). Ellipticity and density at the inner core boundary from subcritical PKiKP and PcP data, *Geophysics. J. Int*., 98: 39-54.

[76]. Shearer, P. & Masters, G. (1990). The density and shear velocity contrast at the inner core boundary, *Geophysics. J. Int*., 102: 491-498.

[77]. Waszek, L. & Deuss, A. (2015b). Anomalously strong observations of *PKiKP/PcP* amplitude ratios on a global scale, *J. Geophys. Res. Solid Earth*, 120.

[78]. Jeanloz, R. & Ahrens, T. J. (1980). Equations of FeO and CaO, *Geophysics. J. R. Astr. Soc.*, 62: 505- 528.

[79]. McQueen, R. G., Marsh, S. P., Taylor, J. W., Fritz, J. N. & Carter, W. J. (1970). *The equation of state of solids from shock wave studies, in high velocity impact phenomena*, Kinslow, R., Academic Press, New York, 294-419.

[80]. Hall, T.H. & Murthy, V. R. (1972). Comments on the Chemical Structure of a Fe-Ni-S Core of the Earth, *EOS*. 53 (5): 602.

[81]. Derr, J.S. (1969). Internal Structure of the Earth Inferred from Free Oscillations, *J. Geophys. Res.*, 74: 5202-5220.

[82]. Bloxham, J. & Gubbins, D. (1987). Thermal core-mantle interactions. *Nature*, 325: 511-513.

[83]. McFadden, Phillip L. & Merrill, R. T. (1995). History of Earth's magnetic field and possible connections to core-mantle boundary processes. *J. Geophys. Res.*, 100: 307-316.

[84]. Woodhouse, J. H. & Dziewonski, A. M. (1989). Seismic modeling of the Earth's large-scale three-dimensional structure, *Phil. Trans. R. Soc. Lond*. A 328, 291-308.

[85]. Anzellini, S., Dewaele, A., Mezouar, M., Loubeyre, P. & Morard, G. (2013). Melting of Iron at Earth's Inner Core Boundary Based on Fast X-ray Diffraction, *Science*, 340 (6131): 464-466.

[86]. Gubbins, D., Masters, T.G. & Nimmo, F. (2008). A thermochemical boundary layer at the base of Earth's outer core and independent estimate of core heat flux, *Geophys. J. Int.*, 174: 1007-1018.

[87]. Altshuler, L.V. & Sharipdzhanov, L. V. (1971). On the distribution of iron in the Earth, the chemical distribution of the latter. *Bull. Acad. Sci. USSR Geophys. Ser*. 4: 3-16.

[88]. Alboussière, T., Deguen, R. & Melzani, M. (2010). Melting-induced stratification above the Earth's inner core due to convective translation. *Nature*, 466: 744-747.

[89]. Derr, J.S. (1969). Internal Structure of the Earth Inferred from Free Oscillations, *J. Geophysics Res.*, 74: 5202-5220.

[90]. Kaula, W. M., Sleep, N. H. & Phillips, R. J. (1989). More about the Moment of Inertia of Mars, *Geophysical Research Letters*, 16 (11): 1333-1336.
[91]. Ahrens, T. J. (1980). Dynamic Compression of Earth Materials, *Science*, 207: 1035.
[92]. Ringwood, A.E. (1984). The Earth's Core: its composition, formation and bearing upon the origin of the Earth, Proc. R. Soc. A, 395: 1-46.
[93]. Jephcoat, A. & Olson, P. (1987). Is the Inner Core of the Earth Pure Iron? Nature, 325: 332-335.
[94]. Chandler, S. C., 1891. On the variation of latitude, *Astronom. J.* 11, 59-61, 65-70.
[95]. Gross, Richard S. (2000). The Excitation of the Chandler Wobble, *Geophysical Research Letters*, 27 (15): 2329-2332.
[96]. Stokes, G.M. & Michalsky, J. J. (1979). Cygnus X-1, *Mercury* 8: 60.
[97]. Casertano, S., Iben, I. & Shilds, A. (1993).The Hyades Cluster-Supercluster Connection: Evidence for a Local Concentration of Dark Matter, *Astrophysical Journal*, Part 1, 410: 90-98.
[98]. Brady, Joseph L. (1971). The orbit of Halley's Comet and apparition of 1896, *Astronom. J.* 76 (8): 728-739.
[99]. Brady, Joseph L. (1972).The Effect of Trans-plutonian Planet on Halley's Comet. *Publication of the Astronom. Soc. Pacific*, 34 (498): 314-322.
[100]. Flandern, T. V. (1981). The renewal of the Trans-Neptunian planet search, *Bulletin of the American Astronomical Society*, 12: 830.
[101]. Anderson, John, (1988). Planet X - Fact or Fiction? *Planetary Report*, 8 (4): 6-9.

Tables

Table 1. Calculated PREM data using the simplified method.

Level	Radius R	Density ρ	Shell mass M	Moment of Inertia: I	Gravity g	Pressure P
No.	km	g/cm^2	10^{24} g	10^{40} g.cm^2	10^3·cm/s^2	kbar
94	6371.0	1.02000	5973.289	80205.664	981.959	0.000
93	6368.0	1.02000	5971.729	80163.472	982.628	0.301
92	6368.0	2.60000	5971.729	80163.472	982.628	0.301
91	6356.0	2.60000	5955.860	79735.267	983.721	3.368
90	6356.0	2.90000	5955.860	79735.267	983.721	3.368
89	6346.6	2.90000	5942.042	79363.655	984.348	6.051
88	6346.6	3.38076	5942.042	79363.655	984.348	6.051
87	6331.0	3.37906	5915.418	78650.501	984.772	11.242
86	6311.0	3.37688	5881.498	77746.958	985.341	17.897
85	6291.0	3.37471	5847.813	76855.371	985.937	24.552
84	6291.0	3.37471	5847.813	76855.371	985.937	24.552
83	6256.0	3.37091	5789.430	75323.498	987.046	36.197
82	6221.0	3.36710	5731.761	73827.216	988.241	47.843
81	6186.0	3.36330	5674.801	72365.862	989.523	59.490
80	6151.0	3.35950	5618.547	70938.843	990.895	71.140
79	6151.0	3.43578	5618.547	70938.843	990.895	71.140
78	6106.0	3.46264	5545.290	69104.504	992.443	86.533
77	6061.0	3.48951	5472.542	67309.578	994.021	102.070
76	6016.0	3.51639	5400.312	65553.702	995.631	117.752

75	5971.0	3.54325	5328.609	63836.530	997.275	133.580
74	5971.0	3.72378	5328.609	63836.530	997.275	133.580
73	5921.0	3.78678	5245.188	61870.242	998.311	152.315
72	5871.0	3.84980	5161.788	59937.364	999.243	171.384
71	5821.0	3.91282	5078.443	58038.407	1000.070	190.784
70	5771.0	3.97584	4995.188	56173.776	1000.794	210.515
69	5771.0	3.97584	4995.188	56173.776	1000.794	210.515
68	5736.0	3.98399	4937.243	54894.999	1001.293	224.460
67	5701.0	3.99214	4879.884	53644.500	1001.849	238.440
66	5701.0	4.38071	4879.884	53644.500	1001.849	238.440
65	5650.0	4.41241	4789.122	51695.390	1001.046	260.896
64	5600.0	4.44316	4701.095	49838.510	1000.272	283.051
63	5600.0	4.44317	4701.095	49838.510	1000.272	283.051
62	5500.0	4.50372	4527.934	46282.178	998.780	327.772
61	5400.0	4.56307	4358.719	42930.977	997.393	373.027
60	5300.0	4.62129	4193.543	39778.675	996.149	418.809
59	5200.0	4.67844	4032.484	36818.780	995.087	465.113
58	5100.0	4.73460	3875.615	34044.639	994.249	511.936
57	5000.0	4.78983	3722.994	31449.399	993.682	559.281
56	4900.0	4.84422	3574.669	29026.105	993.433	607.151
55	4800.0	4.89783	3430.681	26767.722	993.557	655.550
54	4700.0	4.95073	3291.058	24667.171	994.111	704.504
53	4600.0	5.00299	3155.823	22717.392	995.158	754.016
52	4500.0	5.05469	3024.990	20911.315	996.768	804.113
51	4400.0	5.10590	2898.564	19241.931	999.016	854.820
50	4300.0	5.15669	2776.543	17702.299	1001.988	906.171
49	4200.0	5.20713	2658.919	16285.574	1005.777	958.203
48	4100.0	5.25729	2545.676	14985.041	1010.487	1010.963

Level	Radius R	Density ρ	Shell mass M	Moment of Inertia: I	Gravity g	Pressure P
No.	km	g/cm^2	10^{24} g	10^{40} $g.cm^2$	$10^3 \cdot cm/s^2$	kbar
47	4000.0	5.30724	2436.792	13794.099	1016.234	1064.504
46	3900.0	5.35706	2332.241	12706.303	1023.150	1118.888
45	3800.0	5.40681	2231.989	11715.364	1031.383	1174.188
44	3700.0	5.45657	2135.997	10815.178	1041.100	1230.486
43	3630.0	5.49145	2071.317	10235.887	1048.886	1270.533
42	3630.0	5.49145	2071.317	10235.887	1048.886	1270.533
41	3600.0	5.50642	2044.225	9999.856	1052.492	1287.866
40	3500.0	5.55641	1956.620	9263.582	1065.775	1346.464
39	3480.0	5.56645	1939.595	9125.339	1068.680	1358.335
38	3480.0	9.90349	1939.595	9125.339	1068.680	1358.335
37	3400.0	10.02940	1821.025	8189.719	1051.122	1442.882

36	3300.0	10.18134	1678.502	7123.015	1028.464	1548.038
35	3200.0	10.32726	1542.384	6164.138	l005.050	1652.385
34	3100.0	10.46727	1412.729	5306.115	980.913	1755.720
33	3000.0	10.60152	1289.573	4541.998	956.089	1857.844
32	2900.0	10.73012	1172.922	3864.903	930.611	1958.564
31	2800.0	10.85321	1062.760	3268.068	904.512	2057.694
30	2700.0	10.97091	959.048	2744.899	877.825	2155.056
29	2600.0	11.08335	861.725	2288.994	850.584	2250.478
28	2500.0	11.19067	770.709	1894.191	822.821	2343.794
27	2400.0	11.29298	685.901	1554.580	794.573	2434.847
26	2300.0	11.39042	607.181	1264.538	765.875	2523.487
25	2200.0	11.48311	534.411	1018.739	736.758	2609.572
24	2100.0	11.57119	467.440	812.171	707.265	2692.969
23	2000.0	11.65478	406.100	640.145	677.436	2773.552
22	1900.0	11.73401	350.208	498.303	647.312	2851.205
21	1800.0	11.80900	299.568	382.619	616.944	2925.821
20	1700.0	11.87990	253.973	289.403	586.388	2997.305
19	1600.0	11.94682	213.202	215.291	555.708	3065.572
18	1500.0	12.00989	177.026	151.249	524.988	3130.550
17	1400.0	12.06924	145.204	112.556	494.331	3192.185
16	1300.0	12.12500	117.486	78.802	463.868	3250.438
15	1221.5	12.16634	98.436	58.583	440.212	3293.691
14	1221.5	12.16360	98.436	58.583	440.212	3293.691
13	1200.0	12.77493	93.378	53.640	432.690	3305.677
12	1100.0	12.82501	72.093	34.814	397.560	3359.210
11	1000.0	12.87073	54.279	21.671	362.182	3408.454
10	900.0	12.91211	39.646	12.826	326.595	3453.339
9	800.0	12.94912	27.892	7.132	290.800	3493.806
8	700.0	12.98178	18.714	3.665	254.839	3529.806
7	600.0	13.01009	11.800	1.698	218.713	3561.307
6	500.0	13.03404	6.836	0.684	182.456	3588.295
5	400.0	13.05364	3.503	0.224	146.088	3610.792
4	300.0	13.06888	1.479	0.054	109.653	3628.883
3	200.0	13.07977	0.438	0.007	73.065	3642.820
2	100.0	13.08630	0.055	0.001	36.699	3653.579
1	0.0	13.08848	0.000	0.000	0.000	3655.973

Table 3. Pressure P of the PREM and deviation E of the calculated pressure using the simplified method from the value of P.

Layer	Radius R	Simplified Method P	Pressure of PREM	Deviation E
	km	Kbar	Kbar	
94	6371	0	0	0
93	6368	0.301	0.299	0.006688963
92	6368	0.301	0.303	-0.00660066
91	6356	3.368	3.364	0.001189061
90	6356	3.368	3.37	-0.000593472
89	6346.6	6.051	6.04	0.001821192
88	6346.6	6.051	6.043	0.001323846
87	6331	11.242	11.239	0.000266928
86	6311	17.897	17.891	0.000335364
85	6291	24.552	24.539	0.000529769
84	6291	24.552	24.546	0.000244439
83	6256	36.197	36.183	0.000386922
82	6221	47.843	47.824	0.00039729
81	6186	59.49	59.466	0.000403592
80	6151	71.14	71.108	0.00045002
79	6151	71.14	71.115	0.000351543
78	6106	86.533	86.497	0.000416199
77	6061	102.07	102.027	0.000421457
76	6016	117.752	117.702	0.000424802
75	5971	133.58	133.52	0.000449371
74	5971	133.58	133.527	0.000396923
73	5921	152.315	152.251	0.000420358
72	5871	171.384	171.311	0.000426126
71	5821	190.784	190.703	0.000424744
70	5771	210.515	210.425	0.000427706
69	5771	210.515	210.426	0.000422952
68	5736	224.46	224.364	0.000427876
67	5701	238.44	238.334	0.000444754
66	5701	238.44	238.342	0.000411174
65	5650	260.896	260.783	0.00043331
64	5600	283.051	282.927	0.000438276
63	5600	283.051	282.928	0.00043474
62	5500	327.772	327.623	0.000454791
61	5400	373.027	372.852	0.000469355
60	5300	418.809	418.606	0.000484943
59	5200	465.113	464.882	0.0004969
58	5100	511.936	511.676	0.000508134
57	5000	559.281	558.991	0.000518792
56	4900	607.151	606.83	0.000528978
55	4800	655.55	655.202	0.000531134
54	4700	704.504	704.119	0.000546783
53	4600	754.016	753.598	0.000554672
52	4500	804.113	803.66	0.000563671
51	4400	854.82	854.332	0.000571207
50	4300	906.171	905.646	0.000579697
49	4200	958.203	957.641	0.000586859
48	4100	1010.963	1010.363	0.000593846
47	4000	1064.504	1063.864	0.000601581
46	3900	1118.888	1118.207	0.000609011
45	3800	1174.188	1173.465	0.000616124
44	3700	1230.486	1229.719	0.00062372
43	3630	1270.533	1269.741	0.000623749
42	3630	1270.533	1269.742	0.000622961
41	3600	1287.866	1287.067	0.000620791
40	3500	1346.464	1345.619	0.000627964
39	3480	1358.335	1357.509	0.000608467
38	3480	1358.335	1357.51	0.00060773
37	3400	1442.882	1441.941	0.000652593
36	3300	1548.038	1546.982	0.000682619
35	3200	1652.385	1651.209	0.000712205
34	3100	1755.72	1754.418	0.000742126
33	3000	1857.844	1856.409	0.000772998
32	2900	1958.564	1956.991	0.000803785
31	2800	2057.694	2055.978	0.000834639
30	2700	2155.056	2153.189	0.000867086
29	2600	2250.478	2248.453	0.000900619
28	2500	2343.794	2341.603	0.000935684
27	2400	2434.847	2432.484	0.000971435
26	2300	2523.487	2520.942	0.001009543
25	2200	2609.572	2606.838	0.00104878
24	2100	2692.969	2690.035	0.001090692
23	2000	2773.552	2770.407	0.001135212
22	1900	2851.205	2847.839	0.001181949
21	1800	2925.821	2922.221	0.00123194
20	1700	2997.305	2993.457	0.00128547
19	1600	3065.572	3061.461	0.001342823
18	1500	3130.55	3126.159	0.001404599
17	1400	3192.185	3187.493	0.001472003
16	1300	3250.438	3245.423	0.001545253
15	1221.5	3293.691	3288.502	0.001577922
14	1221.5	3293.691	3288.513	0.001574572
13	1200	3305.677	3300.48	0.001574619
12	1100	3359.21	3353.596	0.001674024
11	1000	3408.454	3402.383	0.001784338
10	900	3453.339	3446.764	0.001907586
9	800	3493.806	3486.665	0.002048089
8	700	3529.806	3522.024	0.002209525
7	600	3561.307	3552.783	0.002399246
6	500	3588.295	3578.894	0.002626789
5	400	3610.792	3600.315	0.002910023
4	300	3628.883	3617.011	0.003282268
3	200	3642.82	3628.956	0.003820383
2	100	3653.579	3636.131	0.004798507
1	0	3655.973	3638.524	0.004795626

Table 6. The data of the Earth planet in the new Earth model.

Le-vel	Radius	Density	Shell mass	Moment of Inertia	Le-vel	Radius	Density	Shell mass	Moment of Inertia
No.	km	g/cm^3	10^{24}g	10^{40} g.cm^2	No.	km	g/cm^3	10^{24}g	10^{40} g.cm^2
94	6371.0	1.02000			47	4000.0	5.30724	108.883	1190.942
93	6368.0	1.02000	1.560	42.192	46	3900.0	5.35706	104.551	1087.797
92	6368.0	2.60000	0.000	0.000	45	3800.0	5.40681	100.252	990.939
91	6356.0	2.60000	15.869	428.205	44	3700.0	5.45657	95.991	900.186
90	6356.0	2.90000	0.000	0.000	43	3630.0	5.49145	64.681	579.291
89	6346.6	2.90000	13.818	371.612	42	3630.0	5.49145	0.000	0.000
88	6346.6	3.38076	0.000	0.000	41	3600.0	5.50642	27.091	236.031
87	6331.0	3.37906	26.623	713.154	40	3500.0	5.55641	87.605	736.274
86	6311.0	3.37688	33.921	903.543	39	3480.0	6.56645	17.025	138.243
85	6291.0	3.37471	33.885	891.587	38	3400.0	5.60987	66.482	524.600
84	6291.0	3.37471	0.000	0.000	37	3300.0	5.66415	79.503	595.032
83	6256.0	3.37091	58.383	1531.873	36	3200.0	5.71843	75.548	532.191
82	6221.0	3.36710	57.669	1496.283	35	3100.0	5.77270	71.647	474.147
81	6186.0	3.36330	56.960	1461.353	34	3000.0	5.82698	67.805	420.694
80	6151.0	3.35950	56.254	1427.019	33	2900.0	5.88126	64.026	371.635
79	6151.0	3.43578	0.000	0.000	32	2800.0	5.93553	60.313	326.765
78	6106.0	3.46264	73.258	1834.339	31	2700.0	5.98981	56.671	285.875
77	6061.0	3.48951	72.748	1794.926	30	2600.0	6.04409	53.104	248.764
76	6016.0	3.51639	72.230	1755.876	29	2500.0	6.09837	49.616	215.223
75	5971.0	3.54325	71.702	1717.172	28	2400.0	6.15264	46.211	185.049
74	5971.0	3.72378	0.000	0.000	27	2300.0	6.20692	42.893	158.036
73	5921.0	3.78678	83.421	1966.289	26	2200.0	6.26120	39.666	133.982
72	5871.0	3.84980	83.400	1932.878	25	2100.0	6.31547	36.534	112.688
71	5821.0	3.91282	83.344	1898.957	24	2000.0	6.36975	33.502	93.955
70	5771.0	3.97584	83.256	1864.631	23	1900.0	6.42403	30.573	77.588
69	5771.0	3.97584	0.000	0.000	22	1800.0	6.47831	27.752	63.398
68	5736.0	3.98399	57.945	1278.777	21	1787.5	6.48509	3.276	7.027
67	5701.0	3.99214	57.359	1250.499	20	1700.0	6.52703	21.757	44.150
66	5701.0	4.38071	0.000	0.000	19	1600.0	6.88649	22.952	41.722
65	5650.0	4.41241	90.762	1949. III	18	1500.0	7.03784	21.027	33.736
64	5600.0	4.44316	88.027	1856.879	17	1400.0	7.09459	18.677	26.231
63	5600.0	4.44317	0.000	0.000	16	1300.0	7.15135	16.321	19.875
62	5500.0	4.50372	173.161	3556.332	15	1221.5	7.17442	11.235	11.924
61	5400.0	4.56307	169.215	3351.201	14	1221.5	9.17442	0.000	0.000
60	5300.0	4.62129	165.176	3152.302	13	1200.0	9.18575	3.636	3.554
59	5200.0	4.67844	161.058	2959.895	12	1100.0	9.23583	15.317	13.547
58	5100.0	4.73460	156.869	2774.141	11	1000.0	9.28155	12.837	9.471
57	5000.0	4.78983	152.621	2595.240	10	900.0	9.32293	10.560	6.383
56	4900.0	4.84422	148.325	2423.294	9	800.0	9.35994	8.491	4.113
55	4800.0	4.89783	143.989	2258.383	8	700.0	9.39260	6.638	2.507
54	4700.0	4.95073	139.623	2100.552	7	600.0	9.42091	5.004	1.423
53	4600.0	5.00299	135.234	1949.779	6	500.0	9.44486	3.596	0.735
52	4500.0	5.05469	130.833	1806.076	5	400.0	9.46446	2.416	0.333
51	4400.0	5.10590	126.426	1669.385	4	300.0	9.47970	1.468	0.124
50	4300.0	5.15669	122.021	1539.631	3	200.0	9.49059	0.755	0.034
49	4200.0	5.20713	117.625	1416.725	2	100.0	9.49712	0.278	0.005
48	4100.0	5.25729	113.243	1300.533	1	0.0	9.49821	0.040	0.000
Total								5,121.820	76,126.841
							Insufficiency	852.380	4,159.559

Table 7. The data of the dark planet in the new Earth model.

Le-vel	Radius R	Density ρ	Mass of shell ΔM	Moment of Inertia ΔI	Le-vel	Radius R	Density ρ	Mass of shell ΔM	Moment of Inertia ΔI
No.	km	g/cm^3	10^{24} g	10^{40} g.cm^2	No.	km	g/cm^3	10^{24} g	10^{40} g.cm^2
45	3700.375	2.70000							
44	3700.000	2.70053	0.174	1.590	22	1800.000	5.40184	22.932	52.388
43	3030.000	2.80006	32.497	291.052	21	1787.500	5.41961	2.7351	5.860
42	3030.000	2.80006	0.000	0.000	20	1700.000	6.64401	8.3321	37.199
41	3600.000	2.84271	13.900	121.102	19	1600.000	6.68619	9.2161	34.931
40	3500.000	2.98488	46.148	387.849	18	1500.000	6.82836	7.3881	27.897
39	3480.000	3.01332	9.181	74.550	17	1400.000	6.97063	6.6931	21.899
38	3400.000	3.12706	36.526	288.220	16	1300.000	6.11271	3.843	16.858
37	3300.000	3.26923	45.106	337.590	15	1221.500	6.22431	9.675	10.269
36	3200.000	3.41140	44.340	312.352	14	1221.500	6.22431	0.000	0.000
35	3100.000	3.55358	43.427	287.389	13	1200.000	6.25488	2.471	2.415
34	3000.000	3.69575	42.376	262.917	12	1100.000	6.39706	10.520	9.304
33	2900.000	3.83792	41.198	239.129	11	1000.000	6.53923	8.968	6.616
32	2800.000	3.98010	39.904	216.189	10	900.000	6.68140	7.604	4.536
31	2700.000	4.12227	38.504	194.231	09	800.000	6.82358	6.138	2.973
30	2600.000	4.26445	37.010	173.370	08	700.000	6.96676	4.881	1.844
29	2500.000	4.40662	35.431	153.693	07	600.000	7.10793	3.743	1.005
28	2400.000	4.54879	33.780	135.269	06	500.000	7.26010	2.736	0.559
27	2300.000	4.69097	32.066	118.145	05	400.000	7.39227	1.871	0.258
26	2200.000	4.83314	30.300	102.346	04	300.000	7.63445	1.167	0.098
25	2100.000	4.97532	28.493	87.885	03	200.000	7.67662	0.605	0.027
24	2000.000	5.11749	26.655	74.754	02	100.000	7.81880	0.227	0.004
23	1900.000	5.25966	24.798	62.933	01	0.000	7.96097	0.033	0.000
Total								852.380	4,159.559